Supplementary information and figures to "The atmospheric river threat to Antarctic Peninsula ice-shelf collapse"

Jonathan D. Wille*, Vincent Favier, Nicolas C. Jourdain, Christoph Kittel, Jenny Turton, Cécile Agosta, Irina V. Gorodetskaya, Ghislain Picard, Francis Codron, Charles Amory, Xavier Fettweis, Juliette Blanchet, Vincent Jomelli

*Corresponding author. Email: jonathan.wille@univ-grenoble-alpes.fr

Contents

More details on the relationship between AR events and ice shelf calving

To examine cooccurrences between AR landfalls and iceberg calving , we utilized the iceberg tracking database from Stuart and Long, 2011 [1]. From this dataset we observe that iceberg calving occurrences largely decreased after 2010 following a similar decrease in AR activity (Supplementary Fig. 7). However, there was difficulty with applying this database as the initial detection of an iceberg on satellite images often occurs many days after the actual calving from the parent ice shelf and in some cases the iceberg origin is unknown sometimes stemming from trapped icebergs in the Larsen B embayment in the years after the collapse. We thus examined calving and collapse events along Larsen A, B and C (between 64.5°S and 68.5°S) using MODIS-Terra and Aqua visible imagery from August-March 2000-2020, and found 21 major calving and collapse events, 13 of which were preceded by an AR landfall within 5 days prior (The Larsen C calving in July 2017 is not considered here as it could not be retrieved during austral winter using MODIS; see Supplementary Data 1). The eight calving events that did meet our criteria (i.e. an AR landfall according to the vIVT detection scheme at least five

days prior to the calving/collapse event) happened under various circumstances. From these eight events, two calving events on February 8 and 23, 2002 occurred within five days of weak AR landfalls only detected by the IWV detection scheme while a third calving event on February 17 occurred with no prior AR detections from the vIVT or IWV schemes. This month was characterized by many calving events whose exact dates of occurrence were difficult to determine as the Larsen B was in a state of near continuous calving and collapse. However, the major final collapse on March 1-2 occurred after an AR landfall detected by the IVT scheme from February 25-27 (see Supplementary Fig. 14) and is counted as one of the 13 linked to ARs.

Two calving events on December 24th, 2001 and February 5th, 2008 were preceded by very intense ARs, but around 10 days prior. The calving event from November 29th, 2004 occurred after a long duration AR event, but also around 10 days prior. Only two calving events showed no relation with AR activity: a winter calving event on August 20th, 2002, and a calving event on January 29th, 2009. See the supplementary tables for more details on how the calving/collapse events were measured. Another interesting note not described in the main text is the majority of the 13 calving/collapse events since 2000 attributed to ARs occurred when cumulative IVT related with AR landfalls since November exceeded 13000-15000 kg m^{-1} s^{-1} also including the collapse of the Larsen A in 1995. Although this result is rather specific to our approach of detecting ARs and measuring maximum IVT.

Further ice-shelf disintegration case studies

In the main text, a few brief examples of AR effects on ice shelf stability and collapses were presented. Here we describe the circumstances surrounding these examples along with describing other AR events along the Antarctic Peninsula (AP).

Larsen A Collapse 1995

The spectacular, surprising collapse of the Larsen A in January 1995 was preceded by repeated retreats starting in the late 1980s [2–5]. The record warm summers in 1986-1987 and 1992-1993 recorded at a nearby weather station were also summers of high AR frequency and likely preconditioned the ice shelf for collapse [6] (Fig. 1a). The literature on this collapse postulates these retreats pushed the Larsen A to a critical limit where a disturbance would initiate a final collapse [3].

As described in the main text, a historically intense AR landfall on January 24th, triggered the final collapse of the Larsen A [5] (Supplementary Fig. 3). Highly anomalous positive 500 hPa geopotential height anomalies during the AR landfall are indicative of a strong blocking ridge similar to the mean blocking patterns observed for all summer AR landfalls (Supplementary Figs. 15 and 16a). This AR landfall was associated with temperatures well above 0 °C aided by a very large sensible heat flux with very little mitigation from the latent heat flux along with an elevated downward longwave radiative flux resulting in intense surface melt and runoff (Supplementary Fig. 9a). The combination of this very large runoff total, the absence of a regional sea ice cover allowing a swell-induced strain, along with the wind strain associated with the AR were likely the factors that led to the Larsen A ice shelf's dramatic demise [7].

Larsen B Collapse 2002

The same AR that triggered the final collapse of the Larsen A also caused the calving of a large tabular iceberg (~1700 km^2) along with smaller icebergs (~550 km^2) from the front of the Larsen B, which had been growing in size until early 1995 [5]. After the January 1995 AR, the Larsen B experienced a period of high melt years and above-average AR activity, especially in summer 1999/2000 [8], that preconditioned the ice shelf for collapse. As discussed in the main text, unlike the collapse of the Larsen A in 1995 where a single AR landfall could be linked with the final collapse, several AR landfalls preceded in the months before the final collapse of the Larsen B in late February 2002. A small area of melt ponds was present on the Larsen B near the base of mountains on December 9th that expanded after an intense made landfall on December 13th (Supplementary Fig. 1). MODIS satellite imagery captured a foehn wind clearing out clouds over the leeward Larsen B ice shelf (Supplementary Fig. 1b). The moist incoming flow transitions to broken turbulent clouds over the Larsen B with enhanced sensible heat flux and downward longwave radiation (Supplementary Figs. 1b and 9b). Afterwards, another intense long duration AR occurred from December 31 - January 2 (Supplementary Fig. 2). This storm had a similar structure as the storm just two weeks earlier with a cloud band extending from east of South America to the AP (Supplementary Fig. 2b). A day after the AR passed, increased swells likely added strain to the ice-shelf margins in the absence of a sea ice cover [7] (Supplementary Fig. 2e). These two AR landfalls were associated with the two highest

92 temperature periods during the month of December 2001, while the winds during December 13th
93 were particularly intense averaging ~20 m s^{-1} (Supplementary Fig. 9b).
94 Throughout February, the Larsen B was in the process of rapidly destabilizing with melt
95 ponds and crevasses appearing more clearly while large icebergs were filling the embayment.
96 Between the IWV and vIVT AR detection schemes, three distinct AR landfalls were detected
97 (04/02, 18/02, and 25/02) although the two schemes did not agree on the first two events. This
98 series of moderately intense ARs likely exacerbate the ongoing collapse with further melting and
99 wind stress. The AR that preceded the major breakup of the Larsen B in the beginning March
100 occurred from February 25-27 (in the 81.5th intensity percentile) and generated 2.4 Gt (2.9 Gt)
101 of runoff (meltwater) with a further southward melt extent then the previously documented AR
102 landfalls that summer (Supplementary Fig. 14). Like the previous AR landfalls, anomalously
103 large swells were apparent along the ice-shelf margin (Supplementary Fig. 14e). Each of the
104 three February AR landfalls were associated with temperatures above 0 °C, high wind velocities,
105 and elevated sensible heat and downward longwave radiative fluxes (Supplementary Fig. 9c); all
106 patterns described in the main text as potentially destabilizing. The summer of 2001/2002 was
107 characterized by persistent atmospheric blocking centered slightly northeast of the AP tip that led
108 to a predominantly NE and NW flow advecting warm moist air masses [9] and directing ARs
109 towards the AP (Supplementary Figs. 16b and 16c).
110
111 *Larsen C/Scar Inlet ice shelf*
112 While the Larsen A and B have mostly disintegrated during the 21st century, the Larsen
113 C remains in a stable configuration [10]. Recently though, the calving of a large tabular iceberg
114 (~6,000 km^2) on July 12th, 2017 brought the stability of the remaining Larsen C into question [11].
115 The crack leading to the calving, which had been growing over the course of many years,
116 appears related to basal melting from subsurface melting [12,13]. The ice lost during the massive
117 calving event is believed to be the passive shelf ice supposedly meaning no changes in the
118 buttressing effect and ice-shelf velocity are anticipated [14]. However, the ice-shelf front now
119 displays a concave shape just as the Larsen A and B exhibited prior to their break-ups [14,15] and
120 any further calving could have a destabilizing effect. In addition, the Larsen C is sensitive to the
121 same AR-related mechanisms that drove the preconditioning and final collapses of the Larsen A

and B (i.e. foehn winds, hydrofracturing, swell-induced strain). Even during winter temperatures above 10 °C have been measured on the Larsen C during foehn wind events [16].

Following the Larsen B ice shelf disintegration in 2002, the shelf ice was replaced with land-fast ice while the glaciers that originally fed the Larsen B became tidewater glaciers with increasing velocity [17,18]. The remnants of the Larsen B (named Scar Inlet ice shelf) experienced a 2-3 fold increase in velocity from the loss of back stress after the Larsen B collapse [19]. The land-fast ice in the Larsen B embayment buffers the Scar Inlet from swells [20], but this ice is displaceable contrary to shelf ice. A few AR-related calving events have already been observed on the northern edges of the Larsen C. In early January 2005, an iceberg calved off the NE edge of the Larsen C after an AR landfall (Max IVT ~ 460 kg m^{-1} s^{-1}, in the 83.4th intensity percentile) on January 3rd. Melt pond formation was observed on the interior of the ice shelf near the base of the mountains and extensive runoff occurred throughout the Larsen C with a total 5-day runoff (meltwater) of 5.9 Gt (6.8 Gt) (Supplementary Fig. 17). The next month, a more intense AR (Max IVT ~ 860 kg m^{-1} $s^{-1,}$ in the 99.7th intensity percentile) made landfall February 9th - 10th generating 4.5 Gt (5.0 Gt) of runoff (meltwater) (Supplementary Fig. 12). The sea ice was blown away from the ice-shelf front and another iceberg calved off the ice-shelf front not far from the location of the previous calving. The 500 hPa geopotential height anomalies during the AR show a blocking ridge centered on the northern extent of the AP in a similar position as the other AR events discussed in this section (Supplementary Fig. 16d).

The front of the Scar Inlet ice shelf retreated significantly following two large calving events during the summers of 2005/2006 and 2007/2008 [20]. We found both these calving events were preceded by AR landfalls. After an AR landfall on February 6th - 8th, 2006 (IVT ~ 520 kg m^{-1} s^{-1}, in the 91.0th intensity percentile), a newly calved iceberg and extensive melt ponds were observed from MODIS satellite imagery (Supplementary Fig. 18), leading to a 20 km retreat of the Scar Inlet ice shelf. In early February 2008, another calving event led to a 11 km retreat of the eastern region of the Scar Inlet ice shelf [20]. In this case, MODIS satellite imagery showcases a historically intense AR detection (IVT ~ 962 kg m^{-1} s^{-1}, third highest intensity of all AR landfalls in our database) from January 24th - 26th that disintegrated and fragmented nearly all the land fast ice in the Larsen A and B embayments and generated 6.3 Gt (7.2 Gt) of runoff (meltwater) likely leading to the calving a week later (Fig. 2). These calving events on the Larsen C and Scar Inlet from 2005-2008 marked a period of high detected AR activity, but after 2008,

AR activity largely subsided along with occurrences of ice shelf calving on the AP (Fig. 1). However starting in 2015, AR activity began increasing again highlighted by two continental Antarctic temperature records subsequently set by ARs in March 2015 [21] and February 2020 [22,23].

February 2020 temperature record

One illustrative example of an AR's warming capabilities is from February 6th, 2020, when a temperature of 18.3 °C was recorded at Esperanza Base beating the previous record also caused by an AR in March 2015 [21,23]. The AR detected in early February 2020 (detected by the IWV, vIVT, and AR detection scheme in Gorodetskaya et al., 2014), exhibited a very high integrated water vapor content, cloud liquid water, sensible heat fluxes, and downward longwave radiation all resulting in highly anomalous temperatures. A series of AR landfalls (max IVT ~ 486 kg m^{-1} s^{-1} in the 87.5th intensity percentile) directed an extremely moist air mass with supercooled liquid water-laden clouds towards a landfall on the western AP that is perpendicular to the mountain ranges. This led to orographically enhanced precipitation formation, contributing to the stronger foehn winds and sensible heat flux on the leeward ice shelves (Supplementary Fig. 5). The foehn-driven sensible heat flux combined with increased downward longwave radiation from high level clouds generated surface melt on the Larsen ice shelves and surrounding sea ice [22].

Previous large calving events along the Larsen B

ARs landfalls seem to have coincided with many other ice-shelf instability events described in the literature before 2000 [5]. For instance, two ARs landfall on February 9-10 and February 13, 1998 may have generated large melt ponds observed on February 15, 1998 [24]. These melt ponds preceded the significant calving (125 km^2) of the Larsen B in late February 1998 and the disruption of a compressive arch visible on March 23 leading to an increased rate of shelf retreat [5]. Between January 10th and February 1st, 1999, a large calving event (676 km^2) occurred [5], while two AR landfalls occurred on January 11 and January 24. However, due to the uncertainty in the timing of the calving events, we did not include these events in our analysis.

References

1. Stuart, K. M. & Long, D. G. Iceberg size and orientation estimation using SeaWinds. *Cold Regions Science and Technology* **69**, 39–51 (2011).
2. Skvarca, P. Fast recession of the northern Larsen Ice Shelf monitored by space images. *Ann. Glaciol.* **17**, 317–321 (1993).
3. Rott, H., Rack, W., Nagler, T. & Skvarca, P. Climatically induced retreat and collapse of northern Larsen Ice Shelf, Antarctic Peninsula. *A. Glaciology.* **27**, 86–92 (1998).
4. Doake, C. S. M., Corr, H. F. J., Rott, H., Skvarca, P. & Young, N. W. Breakup and conditions for stability of the northern Larsen Ice Shelf, Antarctica. *Nature* **391**, 778–780 (1998).
5. Scambos, T. A., Hulbe, C., Fahnestock, M. & Bohlander, J. The link between climate warming and break-up of ice shelves in the Antarctic Peninsula. *J. Glaciol.* **46**, 516–530 (2000).
6. Rott, H., Skvarca, P. & Nagler, T. Rapid Collapse of Northern Larsen Ice Shelf, Antarctica. *Science* **271**, 788–792 (1996).
7. Massom, R. A. *et al.* Antarctic ice shelf disintegration triggered by sea ice loss and ocean swell. *Nature* **558**, 383–389 (2018).
8. Leeson, A. A. *et al.* Regional climate of the Larsen B embayment 1980–2014. *J. Glaciol.* **63**, 683–690 (2017).
9. van den Broeke, M. Strong surface melting preceded collapse of Antarctic Peninsula ice shelf. *Geophys. Res. Lett.* **32**, L12815 (2005).
10. Glasser, N. F. *et al.* Surface structure and stability of the Larsen C ice shelf, Antarctic Peninsula. *J. Glaciol.* **55**, 400–410 (2009).

11. Hogg, A. E. & Gudmundsson, G. H. Impacts of the Larsen-C Ice Shelf calving event. *Nature Clim Change* **7**, 540–542 (2017).
12. Holland, P. R. *et al.* Oceanic and atmospheric forcing of Larsen C Ice-Shelf thinning. *The Cryosphere* **9**, 1005–1024 (2015).
13. Hutchinson, K. *et al.* Water Mass Characteristics and Distribution Adjacent to Larsen C Ice Shelf, Antarctica. *J. Geophys. Res. Oceans* **125**, (2020).
14. Fürst, J. J. *et al.* The safety band of Antarctic ice shelves. *Nature Clim Change* **6**, 479–482 (2016).
15. Skvarca, P. Changes and surface features of the Larsen Ice Shelf, Antarctica, derived from Landsat and Kosmos mosaics. *Ann. Glaciol.* **20**, 6–12 (1994).
16. Jakobs, C. L. *et al.* A benchmark dataset of in situ Antarctic surface melt rates and energy balance. *J. Glaciol.* **66**, 291–302 (2020).
17. Scambos, T. A. Glacier acceleration and thinning after ice shelf collapse in the Larsen B embayment, Antarctica. *Geophysical Research Letters* **31**, (2004).
18. Rott, H., Rack, W., Skvarca, P. & Angelis, H. D. Northern Larsen Ice Shelf, Antarctica: further retreat after collapse. *Ann. Glaciol.* **34**, 277–282 (2002).
19. Wuite, J. *et al.* Evolution of surface velocities and ice discharge of Larsen B outlet glaciers from 1995 to 2013. *The Cryosphere* **9**, 957–969 (2015).
20. Qiao, G., Li, Y., Guo, S. & Ye, W. Evolving Instability of the Scar Inlet Ice Shelf based on Sequential Landsat Images Spanning 2005–2018. *Remote Sensing* **12**, 36 (2019).
21. Bozkurt, D., Rondanelli, R., Marín, J. C. & Garreaud, R. Foehn Event Triggered by an Atmospheric River Underlies Record-Setting Temperature Along Continental Antarctica. *Journal of Geophysical Research: Atmospheres* **123**, 3871–3892 (2018).

22. Bevan, S., Luckman, A., Hendon, H. & Wang, G. The 2020 Larsen C Ice Shelf surface melt is a 40-year record high. *The Cryosphere* **14**, 3551–3564 (2020).
23. Xu, M. *et al.* Dominant role of vertical air flows in the unprecedented warming on the Antarctic Peninsula in February 2020. *Communications Earth & Environment* **2**, 133 (2021).
24. Scambos, T. Images of Antarctic Ice Shelves. (2001) doi:10.7265/N5NC5Z4N.
25. Gorodetskaya, I. V. *et al.* The role of atmospheric rivers in anomalous snow accumulation in East Antarctica. *Geophysical Research Letters* **41**, 6199–6206 (2014).
26. Gorodetskaya, I. V., Silva, T., Schmithüsen, H. & Hirasawa, N. Atmospheric River Signatures in Radiosonde Profiles and Reanalyses at the Dronning Maud Land Coast, East Antarctica. *Adv. Atmos. Sci.* **37**, 455–476 (2020).
27. Hubbard, B. *et al.* Massive subsurface ice formed by refreezing of ice-shelf melt ponds. *Nature Communications* **7**, 11897 (2016).
28. Turton, J. V., Kirchgaessner, A., Ross, A. N. & King, J. C. The spatial distribution and temporal variability of föhn winds over the Larsen C ice shelf, Antarctica. *Q.J.R. Meteorol. Soc.* **144**, 1169–1178 (2018).

Supplementary Figures

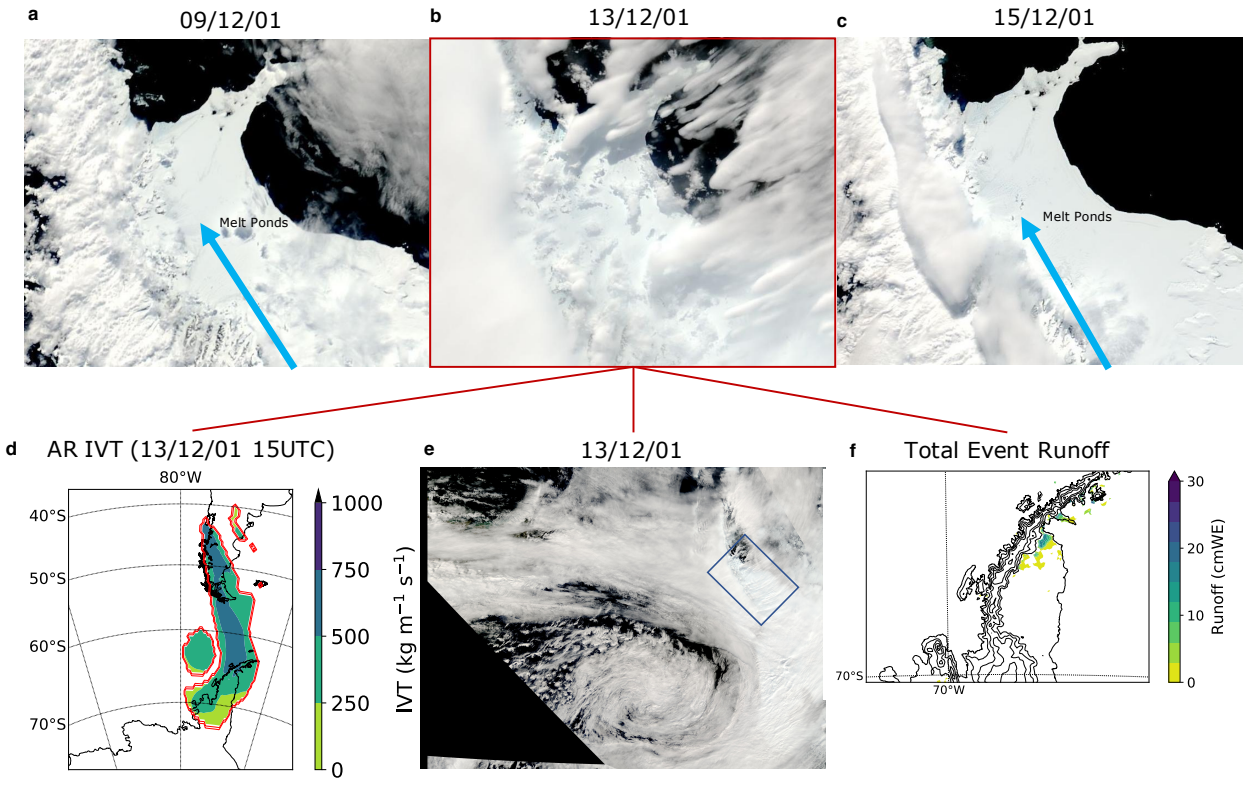

Supplementary Figure 1.

Overview of December 13th, 2001, AR over the Larsen B. MODIS satellite imagery from a 9/12/01, **b** 13/12/01, C 15/12/01 showing the enhanced melt ponds after the passing of an AR. **d** the shape and intensity of the detected AR on 13/12/01 15 UTC and seen in **b** and **e**. **e** An expanded satellite image demonstrating the structure of the AR landfall in 13/12/01. **f** The total runoff that occurred from 9/12/01 - 15/12/01.

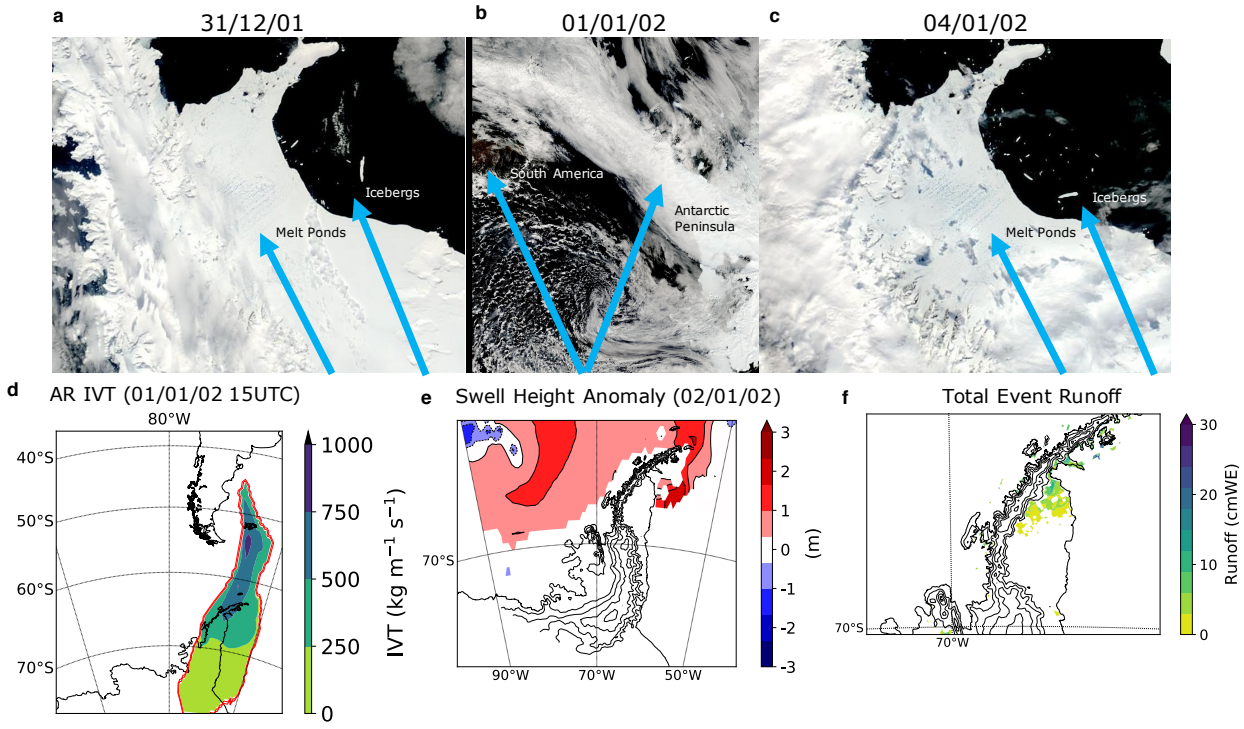

Supplementary Figure 2.

Overview of January 1st, 2001, AR over the Larsen B. MODIS satellite imagery from **a** 31/12/01, **b** 01/01/02, **c** 04/01/02 showing the enhanced melt ponds after the passing of an AR. **d** the shape and intensity of the detected AR on 01/01/02 15 UTC and seen in **b**. **e** The swell height anomalies on 02/01/02 compared to the monthly climatological mean. **f** The total runoff that occurred from 31/12/01 - 04/01/01.

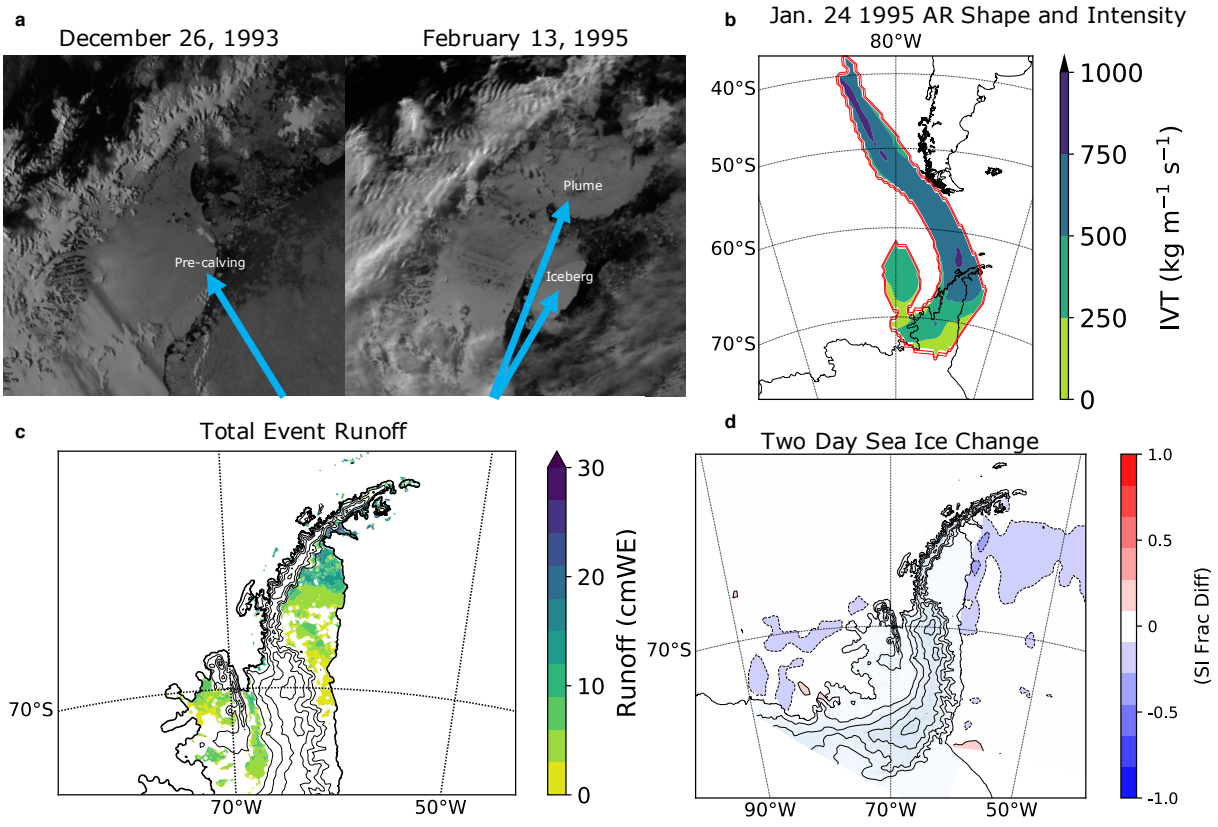

288

289 **Supplementary Figure 3.**

290 Overview of the Larsen A collapse in 1995. **a** AVHRR satellite imagery showing the state of the
291 Larsen A before and after the collapse in late January 1995. **b** the shape and intensity of the
292 detected AR believed to initiate the final collapse. **c** The total runoff that occurred from 23/01/95
293 00 UTC - 28/01/95 00 UTC. **d** The two-day sea ice change centered on the AR occurrence from
294 24/01/95 00 UTC.

295

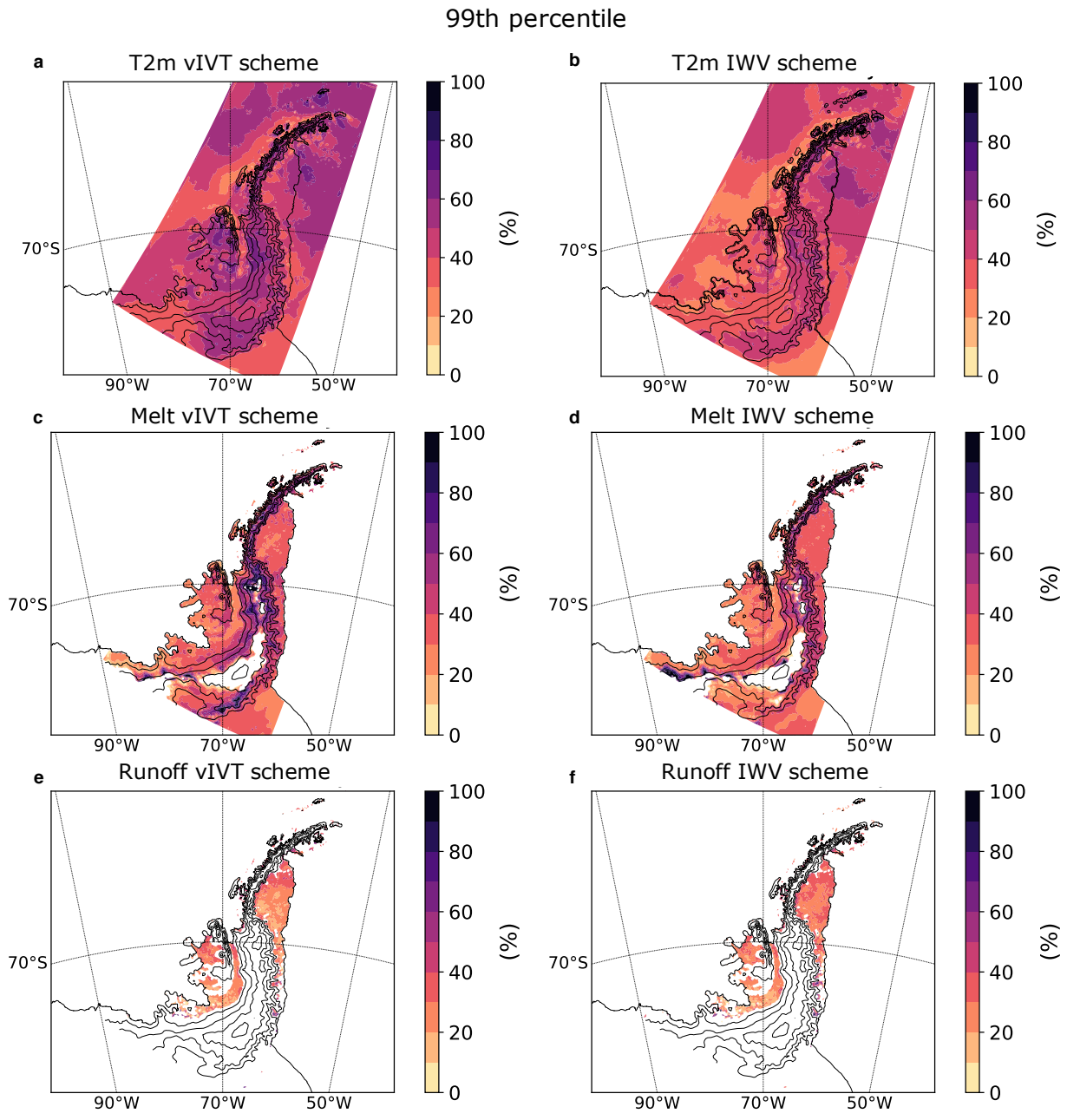

296

297 **Supplementary Figure 4.**

298 The relationship between ARs and extreme temperature, melt, and runoff events. The percentage
299 of MAR **a, b** 2m temperature occurrences, **c, d** surface melt, and e**, f** runoff at or above the 99th
300 percentile of the 1980-2019 climatology that occurred within 24 hours before and after an AR
301 landfall on the AP. **a, b, c** are from the AR climatology generated by the vIVT scheme and **d, e, f**
302 are from the IWV scheme when both are applied to the MERRA-2 reanalysis.

303

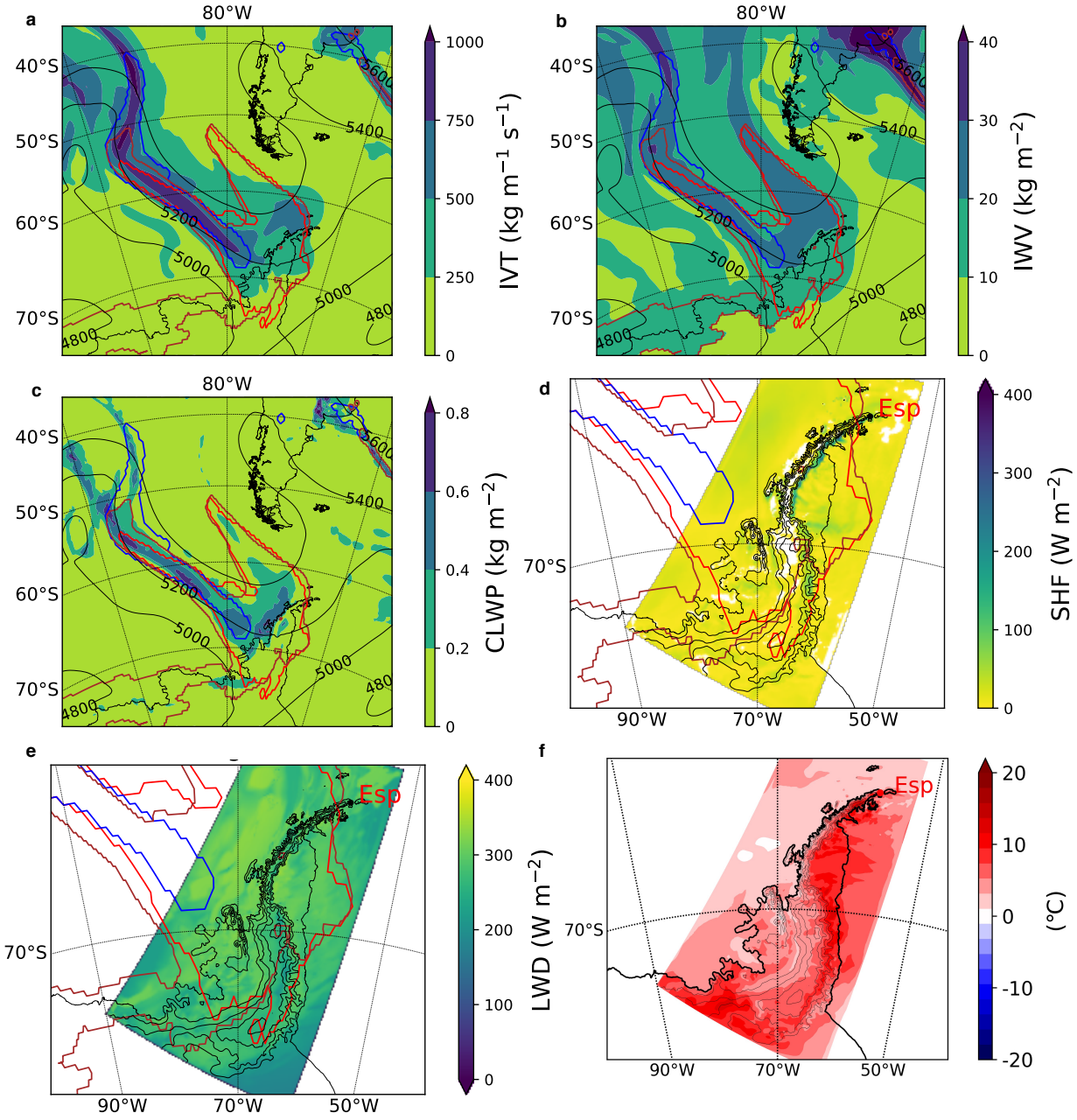

305

306 **Supplementary Figure 5.**

307 The AR shape according to several detection algorithms on 03 UTC 6 February 2020 with spatial
308 distribution of **a** integrated vapor transport (IVT), **b** integrated water vapor (IWV), **c** cloud liquid
309 water path (CLWP), **d** sensible heat flux (SHF), and **e** downward longwave radiation (LWD) all
310 from ERA-5. Contours represent the 500 hPa geopotential height contours in meters. The blue,

red, and brown outlines are the shape of the AR as determined by the vIVT AR detection scheme, IWV AR detection scheme, and the original Antarctic AR detection algorithm respectively [25,26] (Gorodetskaya et al. 2014; 2020). **f** 2m temperature anomalies from MAR on 6 February 18UTC with respect to the 1980-2019 climatology.

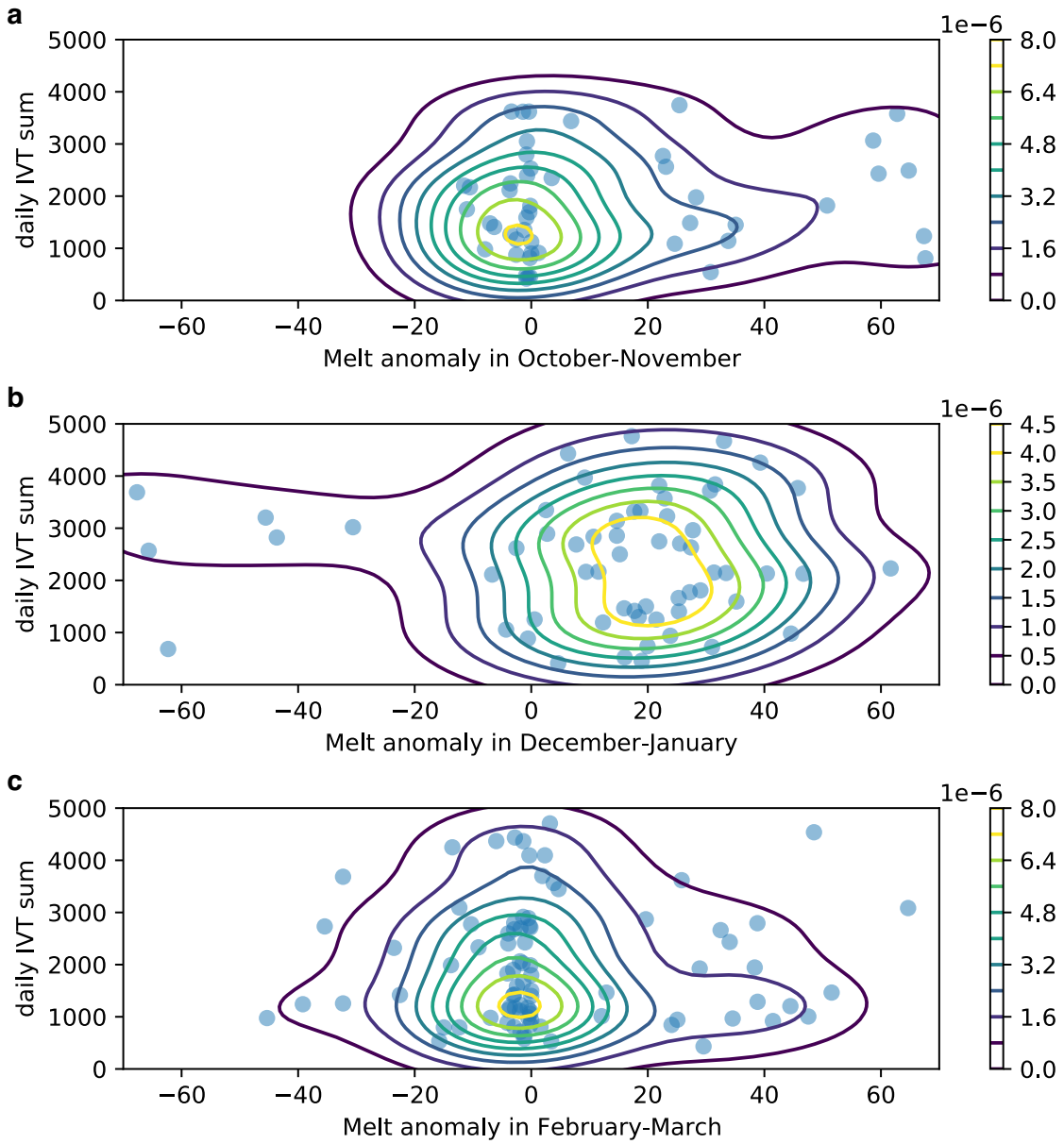

Supplementary Figure 6.

Daily melt surface anomalies over the Larsen C ice shelf during ARs as a function daily IVT values between 1980 and 2021. Melt surfaces were obtained using a series of microwave radiometers (SMMR, SSM/I and SSMIS). Daily melt extent anomalies are relative to a daily melt surface climatology based on mean values for each Julian day mean computed over the full 41 year-long period. Dots are punctual daily anomalies and lines are kernel density distributions for **a** October-November, **b** December-January, and **c** February-March.

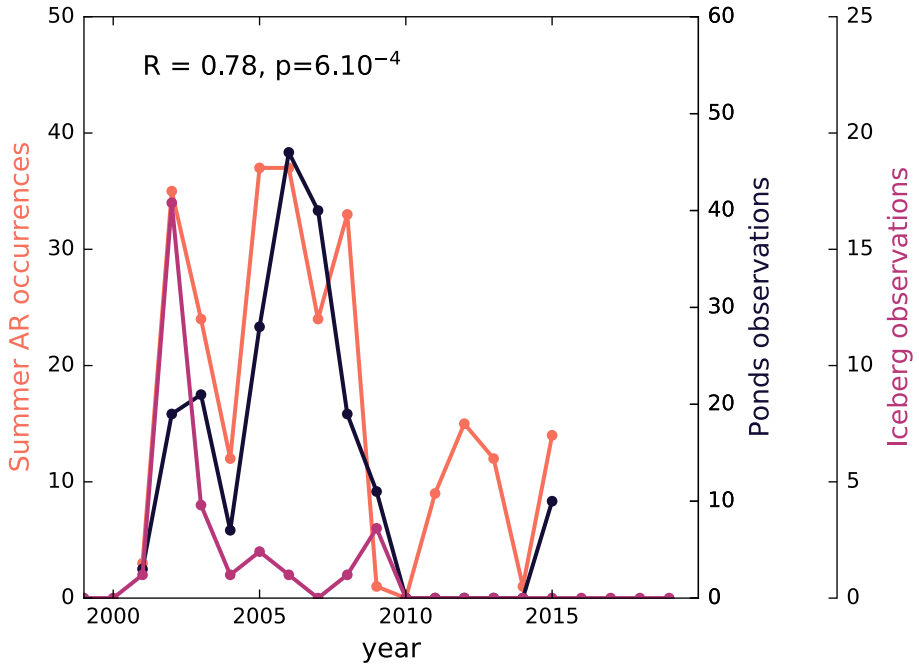

Supplementary Figure 7.

Comparison between the number of summer (DJF) AR 3-hourly occurrences and melt pond and no melt pond observations. r = 0.78 between summer AR occurrences and melt pond observations. Iceberg observations are from an analysis of the iceberg database in Stuart and Long, 2011 and refer to the number of new icebergs defined in the database each year along the edge of the Larsen ice shelves. Melt pond observations are from Hubbard et al. 2016 [27].

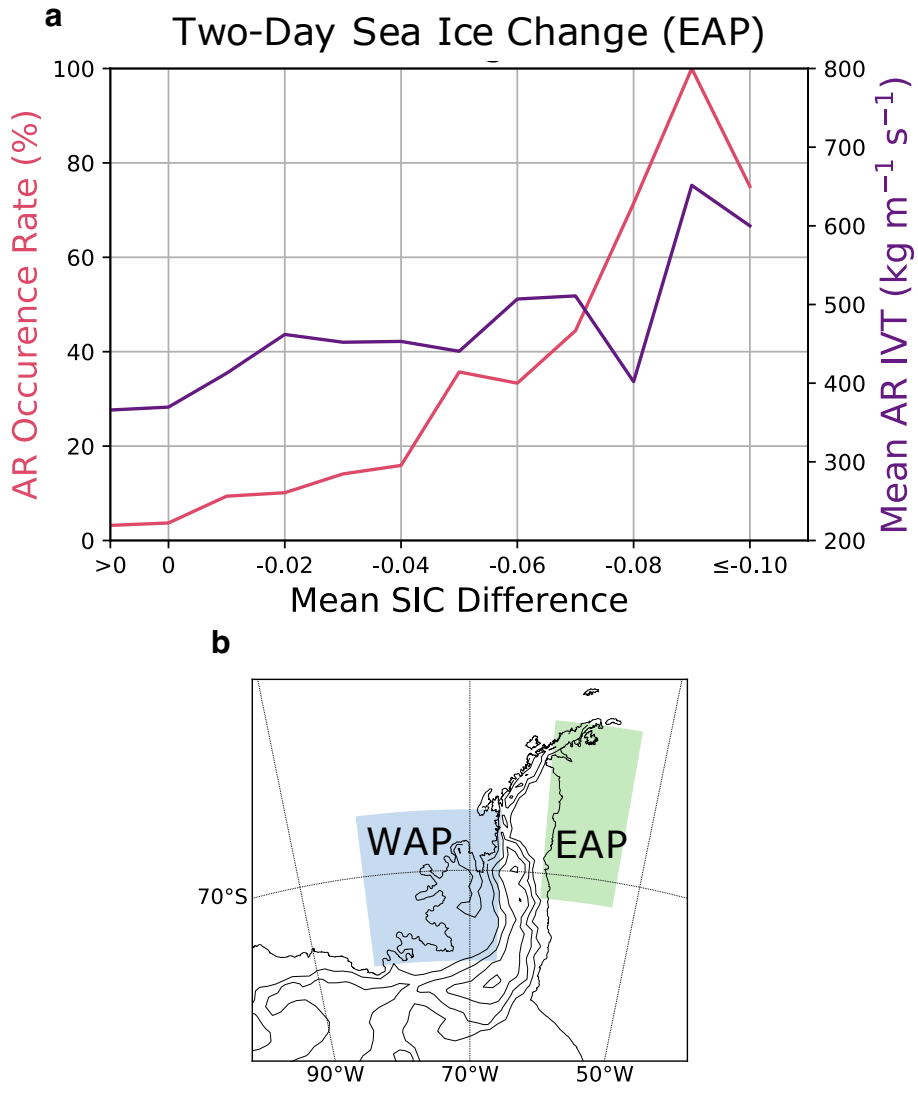

Supplementary Figure 8.

a The percentage of two-day mean sea ice fraction differences associated with an AR landfall on the Antarctic Peninsula in regions east of the Antarctic Peninsula for December-March. The areas considered the East Antarctic Peninsula (EAP is shown in **b).**

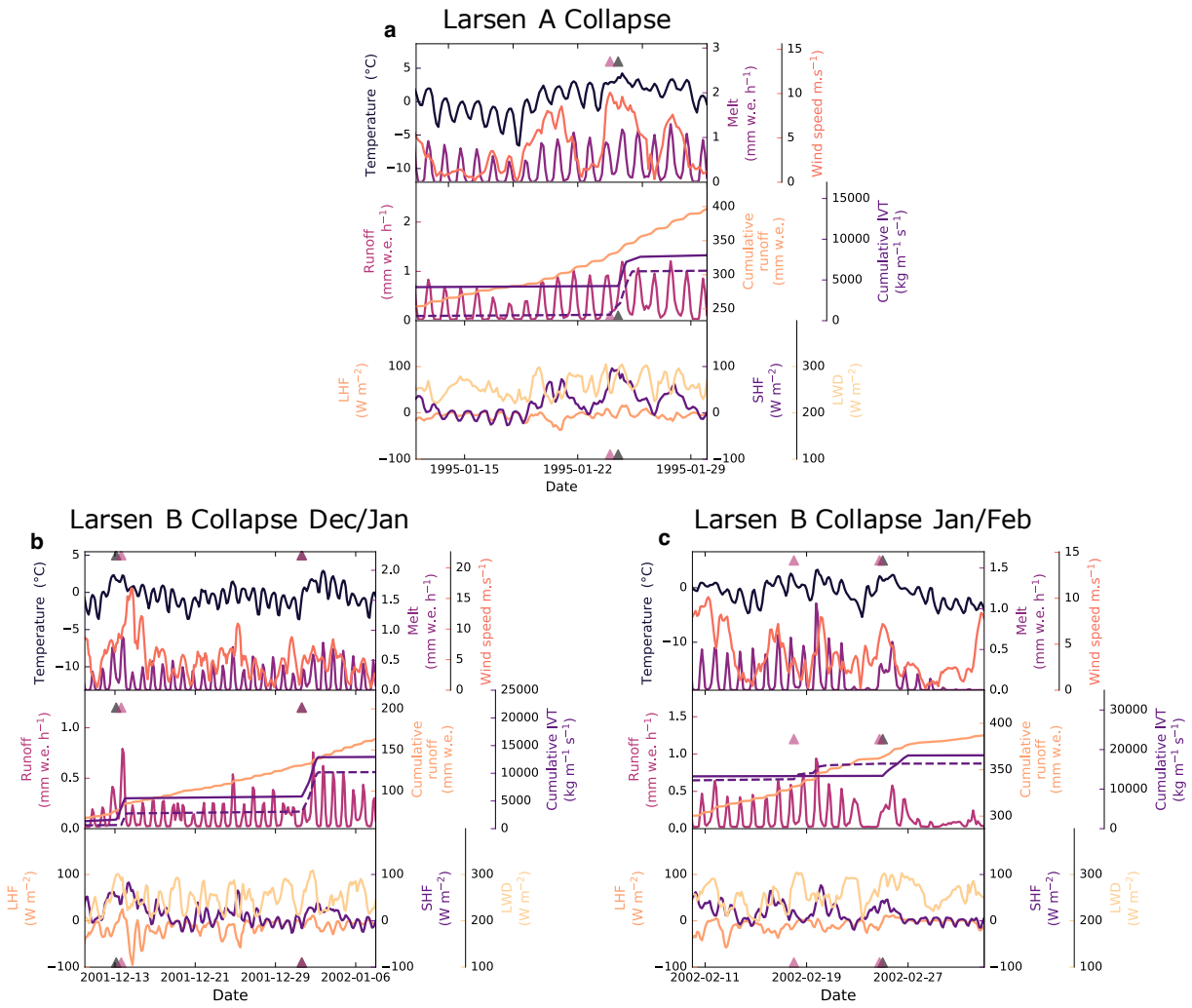

344

345 **Supplementary Figure 9.**

346 Variations of the main meteorological variables during the **a** Larsen A collapse, **b** pre-Larsen B
347 collapse in December/January, and **c** Larsen B collapse in January/February. The date of the first
348 AR detection is displayed with black triangles (for the vIVT scheme) and purple triangles (IWV
349 scheme). The color of the lines refers to the color of the axis of the same panel. LHF is surface
350 turbulent latent heat flux, SHF is surface turbulent sensible heat flux, LWD is downward
351 longwave radiation at the surface. Cumulative runoff and IVT are counted from the previous
352 November. The location of the points used for this analysis are the blue points described in Fig.
353 6c.

354

355

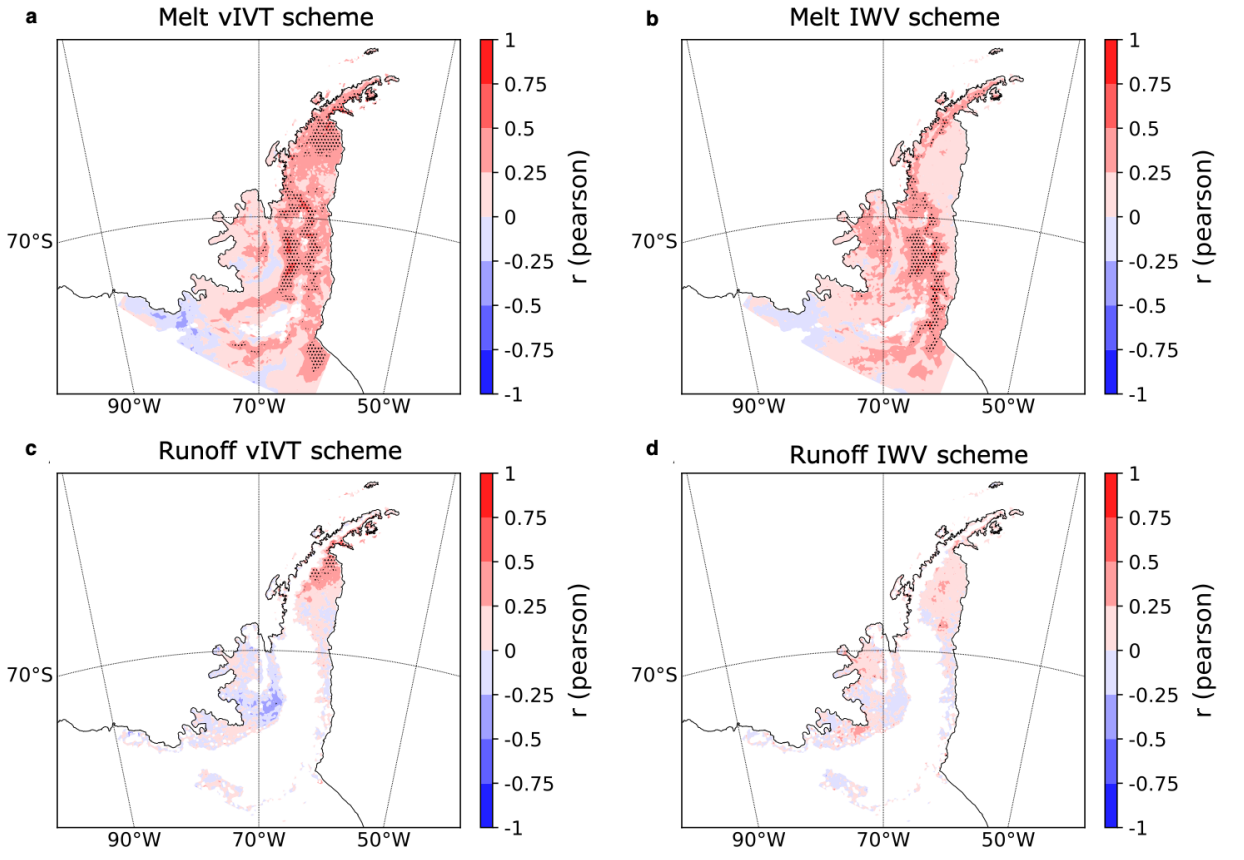

Supplementary Figure 10.

The inter-annual correlations between annual cumulative AR landfall intensity and cumulative **a, b** melt and **c, d** runoff from December-March using the **a, c** vIVT and **b, d** IWV scheme applied to the MERRA-2 reanalysis. Black circles represent areas of significant correlations (p-value < 0.025).

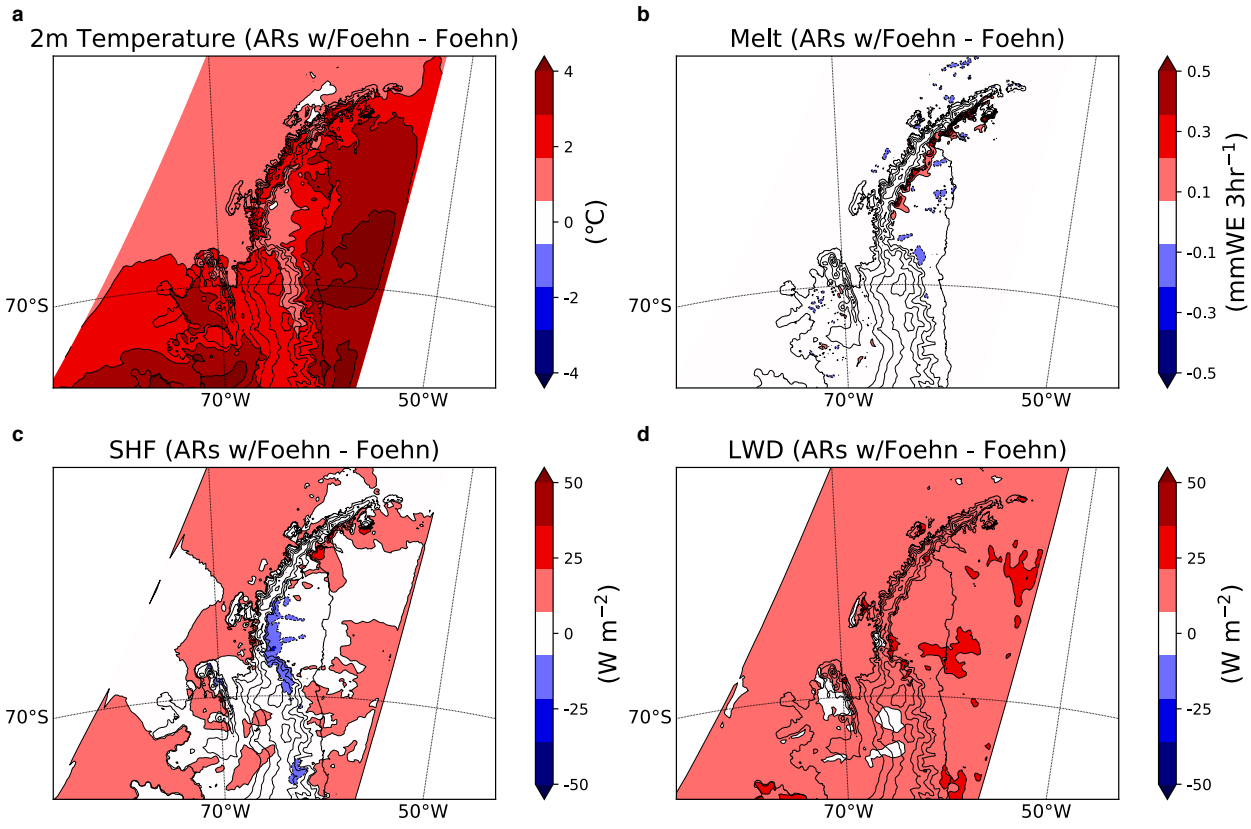

Supplementary Figure 11.

The difference between anomalies associated with ARs cooccurring with foehn winds and foehn wind events according to the algorithm in Turton et al. 2018 [28] for MAR **a** 2m temperature, **b** surface melting, **c** sensible heat flux, and **d** downward longwave radiation from 2009-2012.

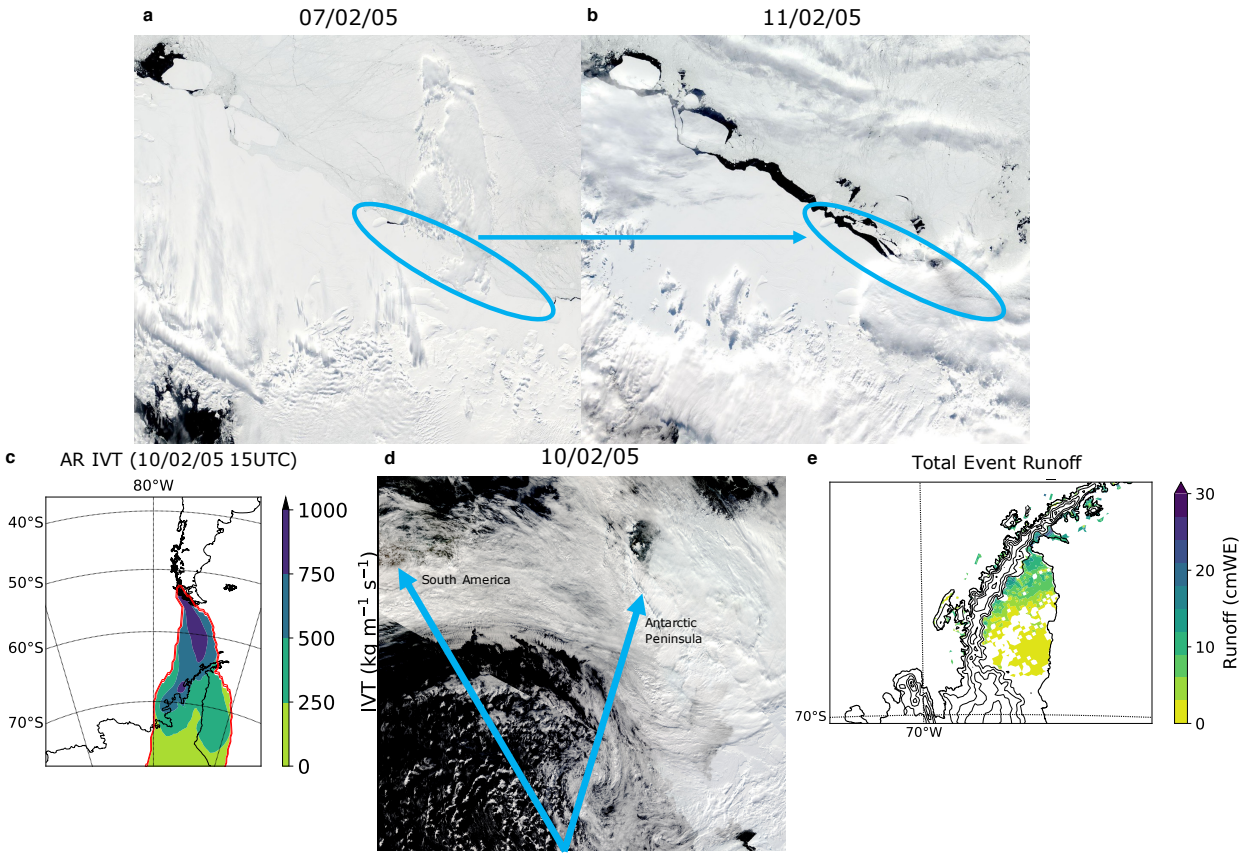

371

372 **Supplementary Figure 12.**

373 Overview of February 10th, 2005, AR over the Larsen C. MODIS satellite imagery from **a**

374 07/02/05 and **b** 11/02/05 showing the calving and sea ice displacement after the passing of an

375 AR as seen in **d** 10/02/05. **c** the shape and intensity of the detected AR on 10/02/05 15 UTC. **e**

376 The total runoff that occurred from 09/02/05 - 14/02/05.

377

378

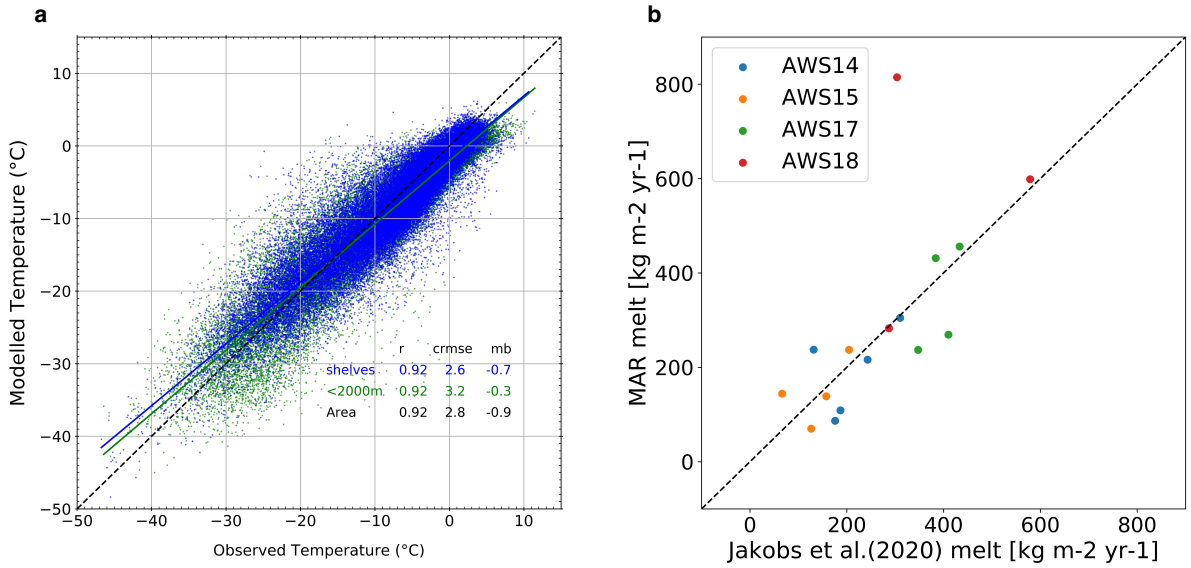

379

380 **Supplementary Figure 13.**

381 **a** Comparison of MAR near-surface temperature modelled to near-surface observed temperature
382 from weather stations over the peninsula between 1981-2018. The comparison is made
383 independently for ice shelves (blue), the grounded ice (all the stations are located below 2000 m)
384 (green), and over the whole area (both ice shelves and grounded ice included). Correlation (r),
385 centered RMSE (crmse) and mean biases are indicated. **b** Comparison of the annual surface
386 melting modelled by MAR to Jakobs et al. 2020 [16] to estimates for four AWS located on the
387 Antarctic peninsula. The locations of the AWS stations are displayed in Fig. 6c.

388

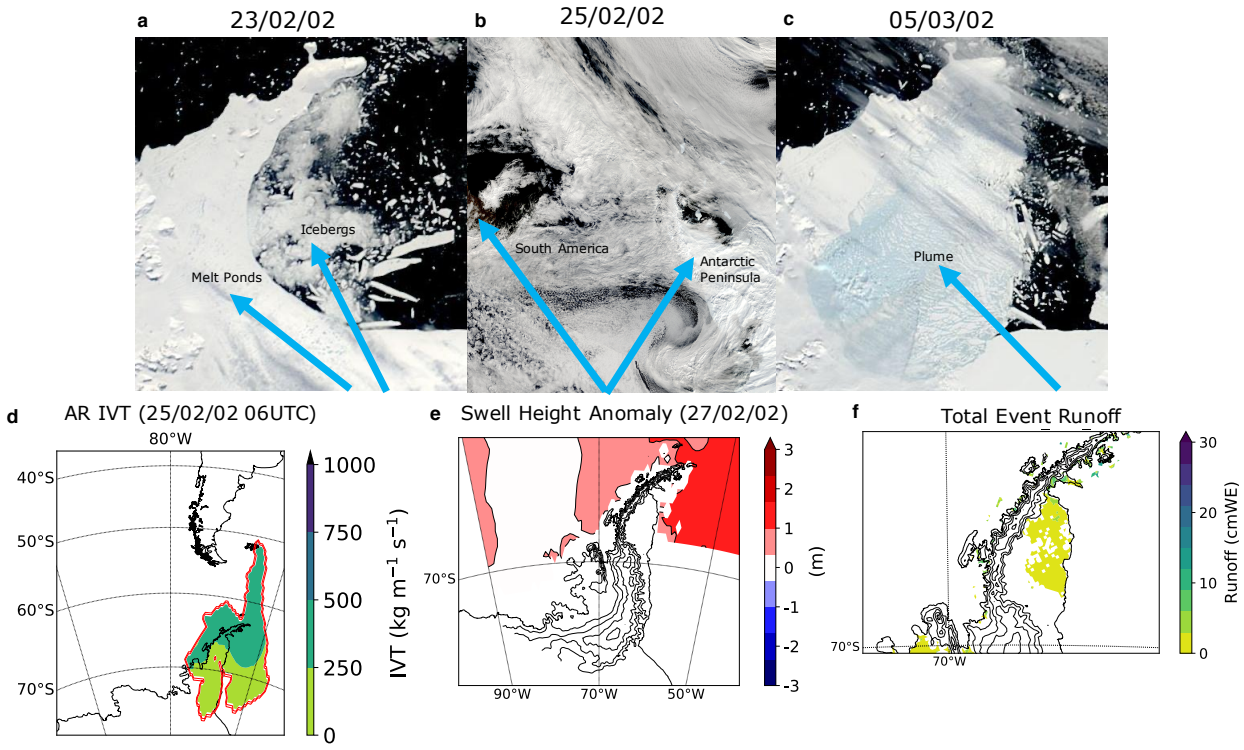

389

390 **Supplementary Figure 14.**

391 Overview of the Larsen B final collapse. MODIS satellite imagery from **a** 23/02/02, **b** 25/02/02,
392 **c** 05/03/02 showing the enhanced melt ponds after the passing of an AR. **d** the shape and
393 intensity of the detected AR on 25/02/02 06 UTC and seen in **b**. **e** The swell height anomalies on
394 27/02/02 compared to the monthly climatological mean. **f** The total runoff that occurred from
395 23/02/02 - 05/03/02.

396

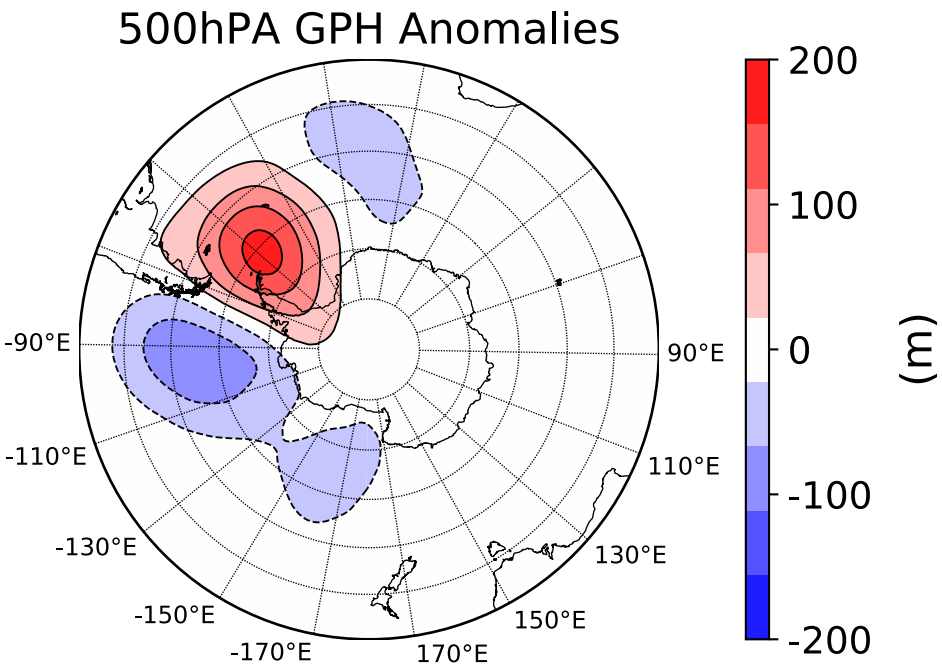

Supplementary Figure 15.

Composite MERRA-2 500 hPa geopotential height anomalies during AR landfalls. Monthly anomalies are with respect to the corresponding climatological monthly mean and then averaged together. The climatology is DJFM 1980-2018.

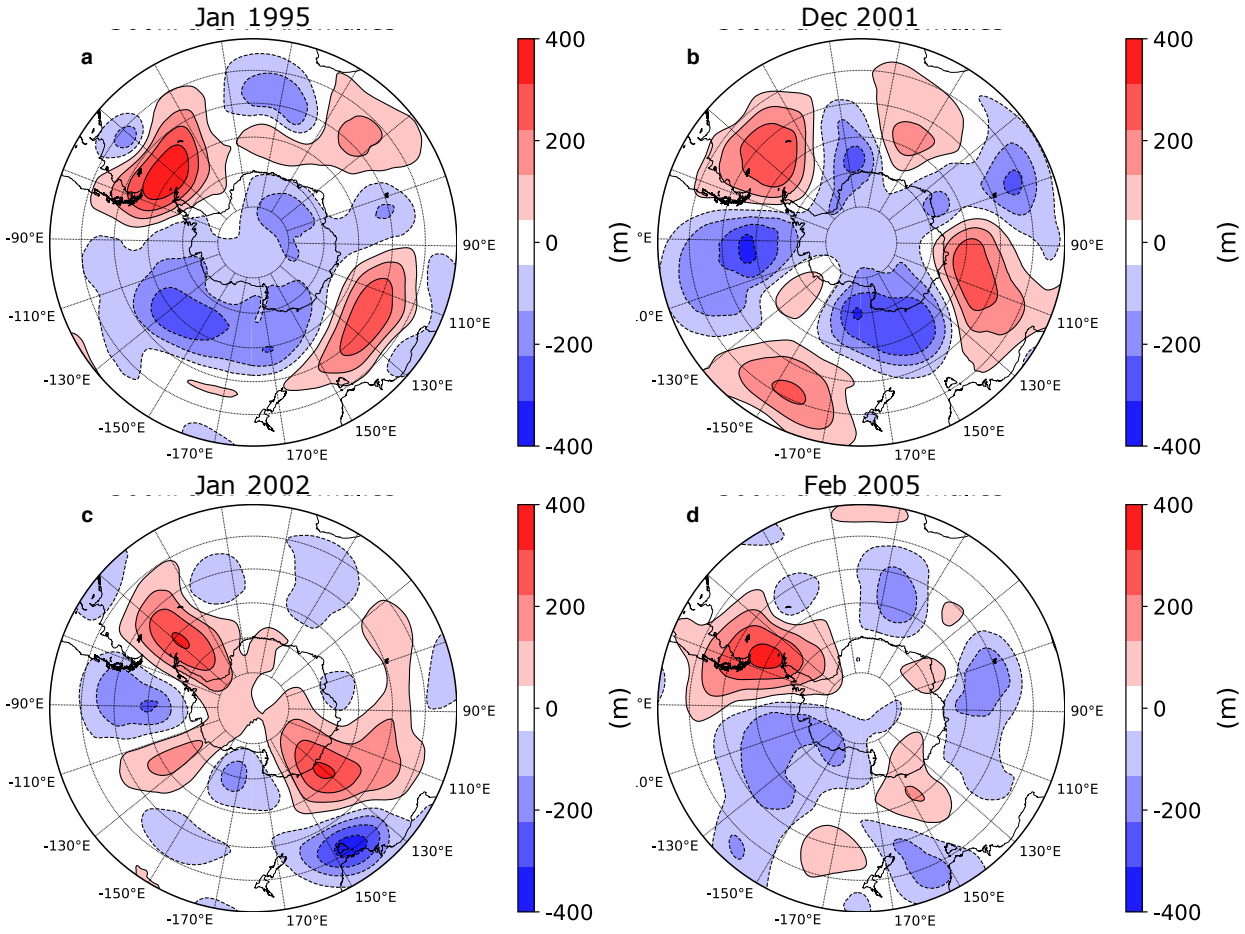

405
406

407 **Supplementary Figure 16.**

408 Composite MERRA-2 500 hPa geopotential height anomalies for **a** 24/01/95 12 UTC - 25/01/95
409 18 UTC, **b** 13/12/01 00 UTC - 14/12/01 00 UTC, **c** 01/01/02 00 UTC - 14/12/01 00 UTC, and **d**
410 09/02/05 18 UTC - 10/02/05 18 UTC. Monthly anomalies are with respect to the corresponding
411 1980-2018 monthly mean.

412
413
414
415

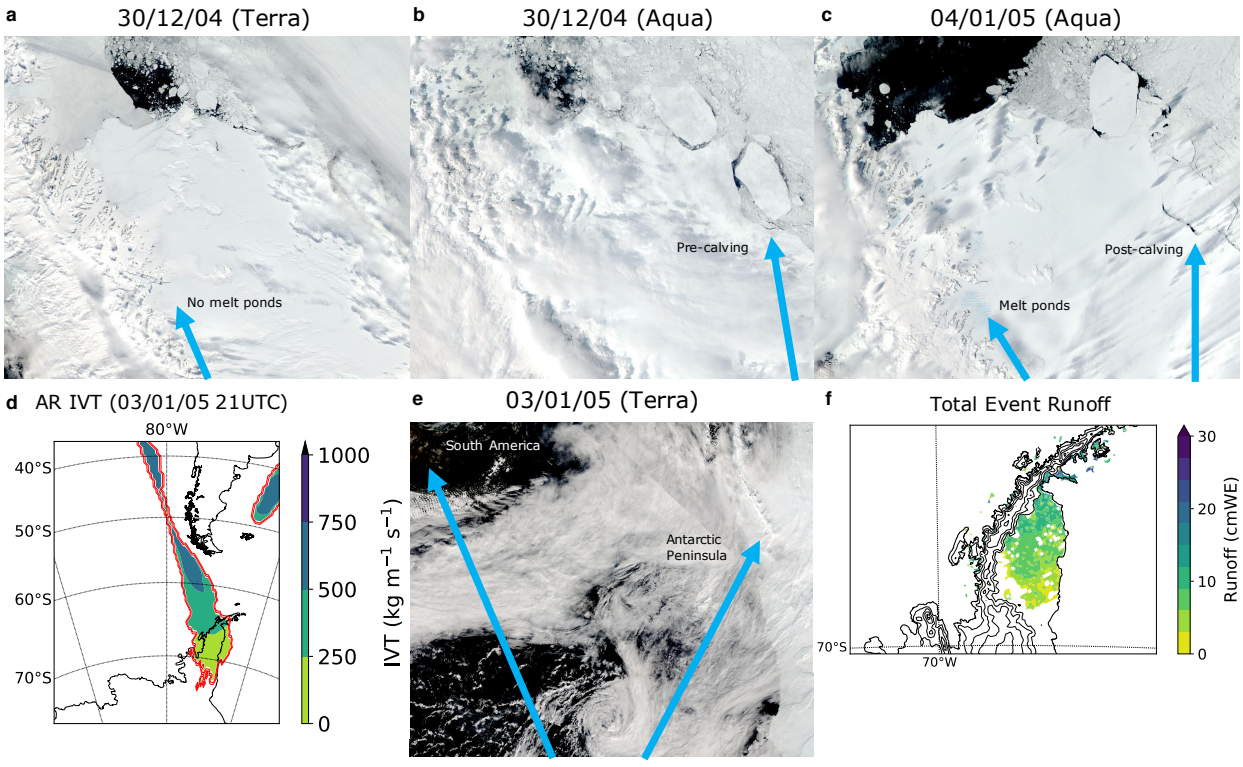

Supplementary Figure 17.

Overview of January 3rd, 2005, AR over the Larsen C. MODIS satellite imagery from **a** 30/12/04 (Terra), **b** 30/12/04 (Aqua), **c** 04/01/05 (Aqua) showing the enhanced melt ponds and calving after the passing of an AR as seen in **e** 03/01/05 (Terra). **d** the shape and intensity of the detected AR on 03/01/05 21 UTC. **f** The total runoff that occurred from 02/01/05 - 07/01/05.

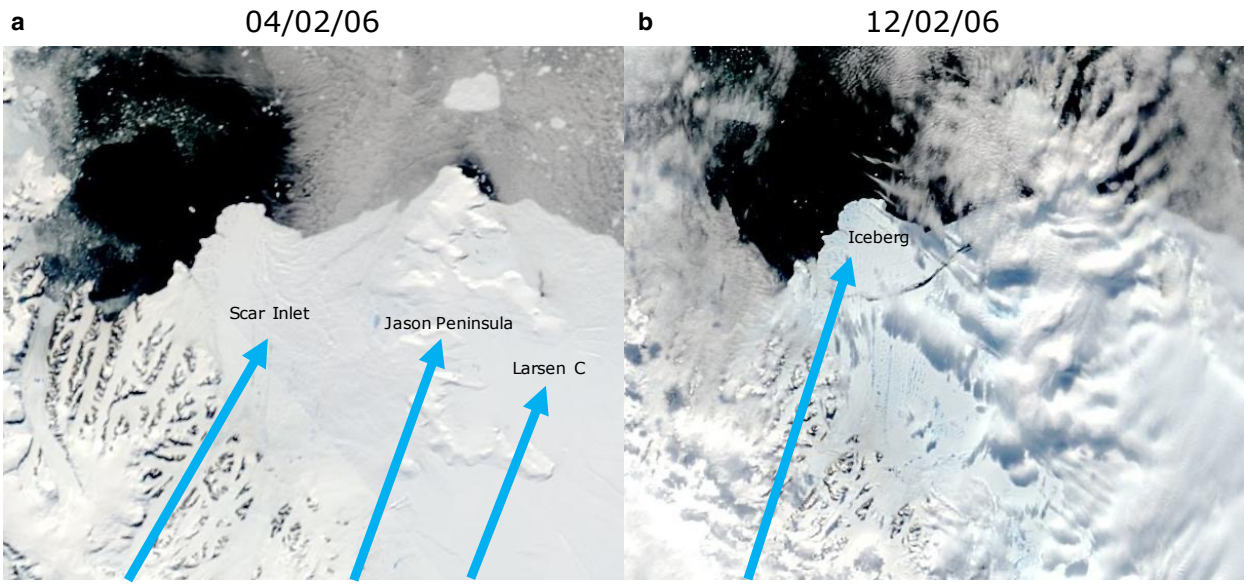

Supplementary Figure 18.

Overview of early February 2006 Scar Inlet ice shelf calving event. MODIS satellite imagery from **a** 04/02/06 and **b** 12/02/06 showing the iceberg calving and melt pond formation following an AR landfall February 6th - 8th.

Year	Number ARs (vIVT)	ARs with foehn (vIVT)	Number ARs (IWV)	ARs with Foehn (IWV)	Number intense ARs (IVT>400)	Intense ARs with Foehn
2009	12	2 (17%)	8	3 (38%)	3	1 (33%)
2010	25	9 (36%)	17	6 (35%)	11	7 (64%)
2011	16	10 (63%)	14	7 (50%)	9	6 (67%)
2012	14	6 (43%)	11	4 (36%)	7	4 (58%)

Supplementary Table 1.

Comparison of ARs detected from the vIVT and IWV detection schemes and foehn events from 2009-2012 using the foehn database described in Turton et al. (2018) [28].

Supplementary Data 1.

Table containing the catalogue of ice shelf disintegration events discussed in the main text.

List of the collapse and calving events retrieved between 68°S and 64.5°S with MODIS images. Names correspond to the nomenclature given in the iceberg database from Stuart and Long (2011) [1].

Index	Collapse date	name
1	2/27/2000	
2	12/24/2001	
3	1/6/2002	
4	2/8/2002	
5	2/17/2002	
6	2/23/2002	
7	3/2/2002	
8	8/20/2002	
9	10/29/2002	a51
10	1/18/2003	a52
11	2/23/2003	
12	4/18/2003	
13	11/29/2004	
14	1/3/2005	a53
15	2/11/2005	
16	1/1/2006	
17	1/20/2006	
18	2/11/2006	a54
19	2/4/2008	a55
20	11/30/2008	uk276
21	1/29/2009	
22	7/10/2017	a68